Swiss Accelerator
Research and
Technology

PSI

HTS Bulk Undulator

PSI – HTS Bulk Undulator

M.Calvi[1], S. Hellmann[2], R. Kinjo[3], X. Liang[1,4], K. Zhang[5].

[1] Photon Science Division, Paul Scherrer institute, Switzerland;

[2] Large Research Facilities Division, Paul Scherrer institute, Switzerland;

[3] Institute of Advanced Energy (IAE), Kyoto University, Gokasho, Uji, Kyoto 611-0011, Japan;

[4] Institute of Biomedical Engineering, ETH Zürich, 8092 Zürich, Switzerland;

[5] Zhangjiang Laboratory, Shanghai, 201210, China.

- x - x - x -

This project has the ambition to demonstrate a new undulator technology with much higher brightness than today status of the art CPMUs[1]. It will potentially push the community to equip the hard X-Ray beamlines of the new Diffraction Limited Storage Rings and future Compact FELs [1] with this new technology on a world-wide impact, as it was the case first for in vacuum undulators. The success of this prototype will require a technology transfer to profit from the expected favourable business case. HTSUs[2] will not only improve and speed up existing activities at the beamlines but they will allow new experiments in medium energy storage rings today possible only in the few large existing facilities, like APS[3], SPring-8[4], ESRF[5] and PETRA III[6].

An example of the application of HTSUs is the technique of total scattering in material science, where a high scattering vector Q is required. With higher photon energies now accessible with an HTSU (40-100 keV), is possible to get large $Q = 4\pi / \lambda \sin\theta$ with relatively small maximum angles (40-60°) and use a frontal area detector for rapid data acquisition [2][3]. In the medium energy range (20-30 keV) presently it is possible to use a 1D detector, with angles larger than 120°, with slow acquisition times but excellent resolution [4]. With the higher flux of the HTSU both at medium and high photon energies, it will be possible to do much faster 1D high-angle acquisitions and even faster acquisitions with frontal 2D. A second high-profile example is undulator-based tomography [5] of high-Z material with dimensions of the order of a few millimetres, where high photon energies and high flux density are required to get through samples of the same order of magnitude linear dimensions. In addition, phase-contrast tomography is required for fast tomography in the 10-100 Hz tomogram rate, which can only be provided by the relatively high coherent fraction offered by undulators.

In the following, the status of the project is reported, divided in six sections: (1) covering the simulation studies, (2) the algorithms developed for the magnetic field optimisation, (3) the magnetic measurement systems, (4) the evolution of the short sample preparation, (5) the results of the short sample measurement campaign and (6) the activities around the development and procurement of the first meter long prototype and its 12 T solenoid and cryostat. Finally, some conclusions are reported, summarising the lesson learned and the status of the advancement of the project.

---

[1] Cryogenics Permanent Magnet Undulators.
[2] High Temperature Superconducting Undulators.
[3] Advanced Photon Source, Lemont, IL 60439 USA.
[4] Super Photon Ring – 8 GeV, Hyogo 679-5198 Japan.
[5] European Synchrotron Radiation Facility, 38043 Grenoble Cedex 9.
[6] At DESY (Deutsches Elektronen-Synchrotron), Hamburg, Germany.

1. Simulation design studies

The specific design of the superconducting staggered array undulator (Figure 1a) requires simulation studies on the magnetisation of the individual HTS blocks. This issue has been tackled in a first attempt with the H-formulation of the Maxwell equations and the commercially available code COMSOL Multiphysics®[7]. This approach has been implemented in collaboration with simulation experts of Karlsruhe Institute of Technology (Grilli and co-workers). This method, well understood and applied successfully to many technical problems, has been for the first time used in the field of undulators [6], with the aim of optimising its performances and better understanding its limits, see Figure 2. New geometries have been proposed and analysed for the first time: like a field enhanced version making use of iron poles Figure 1b and a circular polarised field distribution with a segmented helical geometry (Figure 1c).

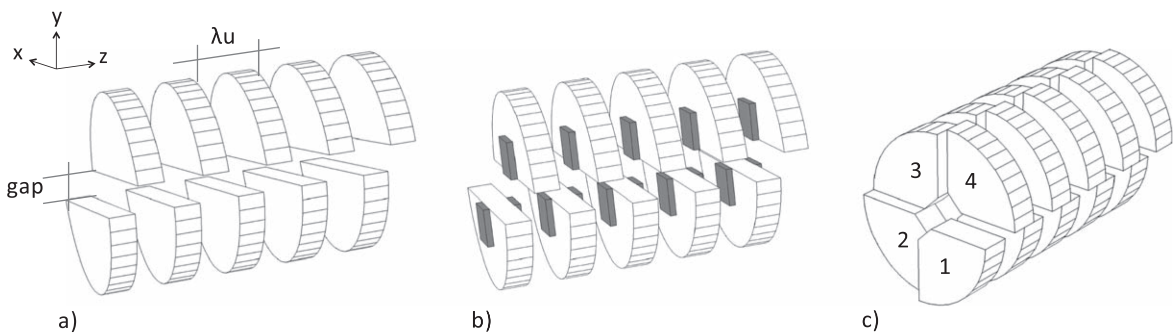

Figure 1 (a) The staggered array undulator geometry as proposed by Kii and co-workers and as it is also implemented in our initial tests. (b) A new hybrid staggered array undulator, where ferromagnetic poles (dark-grey) positioned at the peak undulator field helps increasing its strength. (c) A new helical geometry which extends the staggered array to two dimensions. The round bulks are now cut in four pieces (1, 2, 3 and 4) and relatively shifted of λu/4 along the z-axis.

The H-formulation is widely used to solve transient Eddy-current and magnetization problems in superconductors. The model allows to simulate the magnetization procedure of a staggered array undulator as well as the expected undulator field under the assumption of a given set of geometric undulator parameters and material properties. The geometry of the simulation model presented in Figure 2a shows the full reference geometry of a ten-period staggered array undulator inside a solenoid. To avoid unnecessary overhead in the simulation process, three symmetry planes are used to define a periodic single-period model instead of simulating a larger undulator geometry, see Figure 2b. The single-period model uses a magnetic insulation boundary condition to represent the vertical mirror plane along the electron beam and a perfect magnetic conductor boundary condition to represent the periodicity of the full staggered array undulator. Figure 2c shows the dimensions of the reference geometry of the staggered array undulator. The reference geometry is just a starting point in the optimisation process, which ends up with a different bulk thickness of about 4.0 mm and a new radius of 15 mm (larger does not improve). The magnetic field produced by the solenoid is represented in the single-period model by adding an external magnetic field condition to all external boundaries but the magnetic insulation boundary. During the simulation of the magnetization process the external magnetic flux density is decreased in a linear ramp from 10 T to 0 T in a specified magnetization time.

[7] https://www.comsol.com

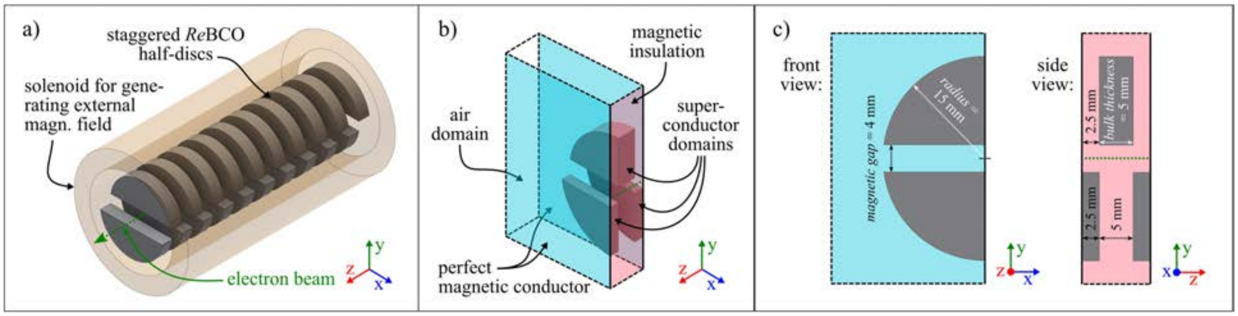

Figure 2 (a) Full geometry of a ten-period staggered array undulator consisting of 20 ReBCO half discs. In the application as an undulator in an electron accelerator the electron beam travels between the upper and the lower row of ReBCO bulks. (b) Simulation model using two symmetries in the model. These are implemented by a magnetic insulation and perfect magnetic conductor boundary conditions. (c) Dimensions of the reference undulator geometry and optimisation parameters radius, bulk thickness and magnetic gap (the depicted sketches are not to scale).

After a preliminary learning period using the H-formulation and COMSOL multi-physics, we proposed new approaches implemented in ANSYS. The first makes use of an iterative algorithm and both the critical state model and the flux creep model have been implemented [7]. The second method is computationally very efficient and is based on the backwards calculation of the critical state model. Indeed, it starts from the eddy current estimation using the A-V method and the algorithm relaxes the solution to comply with the constrains given by the finite *Jc(B,T)* value [8]. These approaches have been compared with the baseline H-formulation, both in terms of accuracy and computational efficiency. The models have been used also to optimise the end field for matching the first and second field integrals, to analyse the experimental data (evaluation of the *Jc* from the field distribution) and to develop a "shimming" strategy. On the latter, a new approach is under investigation which consists of a local variation of the period to compensate the deviation of the peak magnetic field from the target value.

One of the key challenges for designing a long undulator (100 periods or more) is the large-scale simulation of the magnetisation currents inside 200 staggered-array ReBCO bulk superconductors. A feasible approach to simplify the electromagnetic model is to retain five periods from both ends of the 1 m long HTS undulator, reducing the number of DOFs to the scale of millions. The theory of previously proposed 2D backward computation method is extended to calculate the critical state magnetisation currents in the ten-period staggered-array bulk HTS undulator in 3D. The simulation results of the magnetisation currents and the associated undulator field along the electron beam axis are compared with the well-known 3D H-formulation and the highly efficient 3D H-ϕ formulation method, all methods showing excellent agreement with each other as well as with experimental results. The mixed H-ϕ formulation avoids computing the eddy currents in the air subdomain and is significantly faster than the full H-formulation method but is slower in comparison to the A-V formulation-based backward computation. The fastest and the most efficient A-V formulation in ANSYS 2020R1 Academic is adopted to optimise the integrals of the undulator field along the electron beam axis by optimising the sizes of the end bulks. The associated paper has been published in SUST [9].

Recently, we implemented the critical state model with RADIA [10] within a collaboration with ESRF. This approach allows to simulate undulator structure made of many periods (100 or more) within a reasonable time (few minutes). These performances are achieved by neglecting the details of the current distribution within a bulk and assuming a uniform distribution. Presently, this model does not show enough accuracy as a design tool, but it is a very good candidate for implementing advanced data analysis like evaluating the average strength of each bulk out of a magnetic field profile measurement as introduced in the next session.

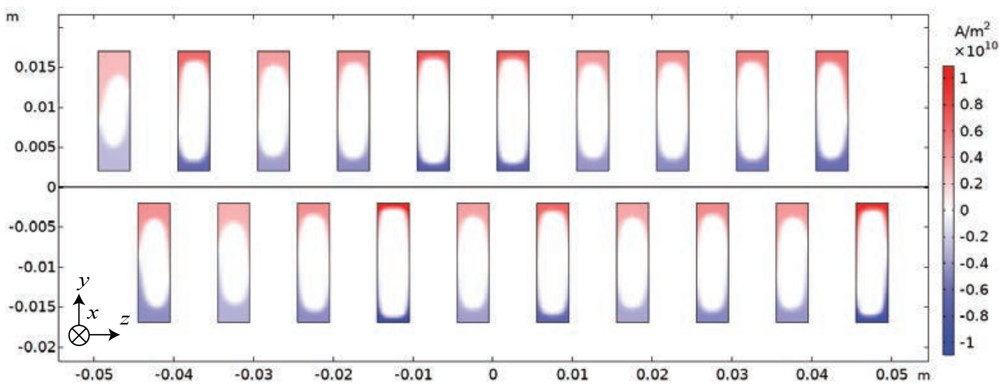

Figure 3 Example of inverse analysis, where the current density distribution is reconstructed starting from a magnetic field profile measurement along a short sample tested at 10K.

2. Optimisation algorithm

Novel algorithms have been developed to extract more information out of the magnetic profile measurements. The most important to be mentioned is the evaluation of the average *Jc* in each crystal [11], see Figure 3. This information allows to sort the disks and reassemble the sample in a configuration where the peak-to-peak pole variation is minimised. Moreover, this technique is more effective the higher the number of disks to be sorted is (if the spread remains constant in the production), allowing an optimistic scaling from 20 disks of the standard short sample to the 200 disks of the first full scale prototype.

The above-mentioned technique shall be used as a course knob to optimise the magnetic field profile and to reduce the spread of the magnetic field amplitude down to a percent, but it cannot provide the final performance expected by the status of the art undulator. This requires achieving values below 0.1 % which call for additional and more refined knobs. For this purpose, pole height tuning and rotation can be used to correct the residual errors in both axes of the transversal plane. These techniques are regularly used in standard undulator and do not present a conceptual problem. Nevertheless, the number of iterations required must be minimised with improved models because each of them require a full thermal cycle, thus it is very time consuming.

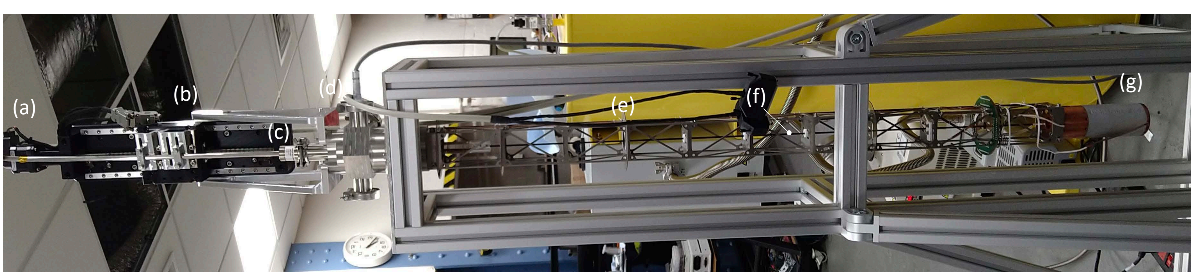

Figure 4 The new magnetic measuring system (rotated of 90°). (a) The stepper motor and incremental rotational encoder (b) linear stage (c) O-ring (d) upper flange equipped with feedthrough and connectors (e) thermal shields (f) the carbon fiber tube supporting the Hall probe (g) the short sample at the bottom.

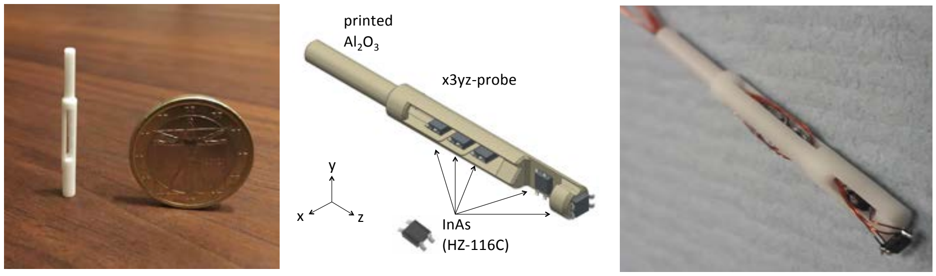

Figure 5 The new ceramic probe 3D printed and equipped with 5 Hall elements to reconstruct the magnetic field vector along the undulator axis while constantly monitoring the vertical alignment (i.e. in the y-axis of the transversal plane).

3. New magnetic measuring system in operation at the University of Cambridge

The installation at the university of Cambridge has been upgraded with a new sample holder. The four long rods which held the sample and thermally isolated it from room temperature, have been substituted with a stainless-steel tube specially machined to reduce its thermal conductivity while keeping a high position accuracy and rigidity to prevent bending in presence of unbalanced magnetic forces, for instance during the quench of an HTS crystal. The vertical installation outside the cryostat is presented Figure 4, where at the bottom (right) the HTS sample is visible. At the top (left), a new stage equipped with an incremental encoder is now used to precisely position the Hall probe along the undulator sample and as well to increase the level of automation of the whole system. This latter was essential to operate the system remotely during the pandemic where only one person was allowed in the laboratory. In this new approach, there are no longer cold connectors, and the wire moves rigidly from the Hall probe up to the warm connector, avoiding any possible collision and damage of the cable with the surrounding cryogenic components. Figure 5 shows the new Hall probe designed, assembled, and calibrated by PSI. Five Hall elements (InAs) are installed, three for the main undulator field (in the picture y-direction): one centred on the axis, the other two respectively one tenth of a millimetre above and below the axis, to permanently monitor the position of the sensor (i.e., the central Hall probe must always measure the lowest field if properly centred). The remaining two Hall elements are for the x- z-component of the field. The x-component shall be ideally zero and it must be measured and corrected in case of deviation. The z-element monitors the solenoidal components during the magnetisation process and evaluates the residual field present at the extremes of the sample, also when the solenoid is fully discharged. A new version of the above probe is under development with the company SENIS, where the Hall elements will be soldered on a flexible PCB and glued on the ceramic support - slightly modified for this purpose) - for a better control of the position and angles. This approach reduces the complexity of the integration and the manual work required and should allow individual powering of the Hall elements (now connected in series) essential for the implementation of the standard spinning current technique (to minimise the Hall planar effect). Additionally, a thermometer will be integrated in the probe, not essential in the vertical rig at Cambridge where the sample is cooled in a stream of helium, but critical for the long prototype working in conduction cooling where the probe will be in vacuum.

Finally, the sample is equipped with two thermometers, one at the bottom and one at the top, and a heater. They are routed through the thermal shields up to the connector and wired to the control system which regulates the temperature of the sample.

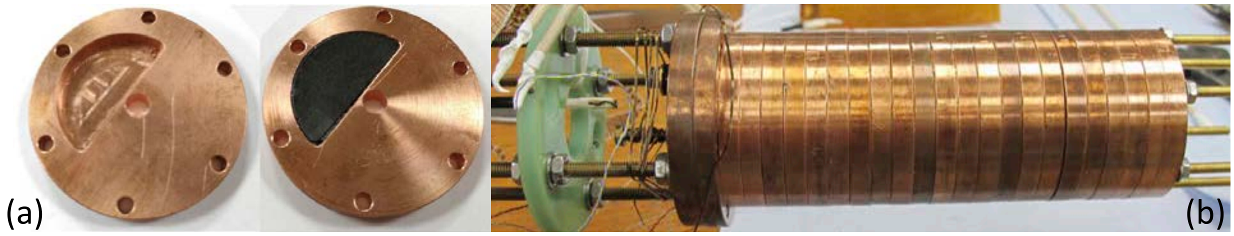

Figure 6 On the left (a) the copper disk alone and the GdBCO crystal machined to its final shape and inserted into the groove of the copper disk. There are six holes on the outer radius for bolting the disks together and a central one for leaving the space required for measuring the field. On the right (b) the second university sample prepared with the nominal length of 10 cm (10 periods) and nominal gap of 4 mm.

4. Sample Preparation

The first two samples tested were prepared at the university of Cambridge and assembled with GdBCO crystals grown and machined in their laboratories. They differ slightly in the geometry but the assembly procedure was the same. The crystals were embedded in a copper sleeve, 5 mm thick, in which a half-moon groove was machined 4 mm deep to lodge the bulk as illustrated in Figure 6a. Finally, epoxy resin was used to permanently fix the crystals to the sleeves and to feel all residual empty spaces, thus avoiding relative movements. The disks were stacked and fixed together by means of six long screws, see Figure 6b. The limits of this assembly are the poor positioning accuracy of the crystals in the copper sleeves and the uncertainty of the relative position between disks. Secondly, the clamping mechanism leaves open the possibility of relative displacement of the disks under the Lorentz force which can generate heat caused by friction and trigger a quench (i.e. a local transition to normal conductivity with thermal run away).

To overcome the above-mentioned limitations – which are probably at the origin of the issues illustrated in the next section – we developed a new assembly procedure. In the following we refer to these samples as industrial sample. This name is justified both because we collaborate with industries for achieving the target mechanical accuracy and because the crystals are also procured at the industrial partners. This time the crystals are embedded into the copper sleeves by mean of thermal expansion: the copper is heated up to 200°C and the REBCO bulks are pressed inside. The cross section of the new sample is presented in Figure 7 where the actual dimensions are quoted in mm. Differently from the university version, the copper disks have now the same thickness of the bulk, 4 mm, because we wanted to avoid problem with the planarity of the structure which would have compromise the accuracy of the assembly. This choice gives the freedom to introduce additional spacers 1 mm thick which could be either made of copper or equipped with additional ferromagnetic material to enhance the magnetic field. This second option was demonstrated to be the most promising one because gives a simple and effective mean to fine tune the magnetic field, exactly in the same fashion as for permanent magnet undulators. Finally, the disks are pressed together and assembled into an external cylinder. By mean of two little "noses" placed at 180 degrees, the azimuthal angle is defined very precisely as well as the gap size. There are three versions of the "cylinder": the first is an actual hallow cylinder made of aluminium installed by thermal expansion; the second and the third ones are made of two half shells bolded together made of aluminium and copper respectively.

The 2D filed map of all industrial HTS disks were, either before or after the short sample test, measured to better understand the undulator field profile. Quickly, it was realised that some disks showed large damage incompatible with this application. This was the case for instance of the two YBCO samples (see section 5.2) which were equipped with many damaged disks. Since then, all disks were measured before assembly.

Figure 7 An example of industrial samples where the ReBCo bulks are machined with Laser Micro Jet (the same is possible with EDM Wire Erosion) and precisely assembled with in a copper matrix with shrink fitting techniques making use of high accuracy machining. Finally, the disks are stacked together and aligned using an external aluminium cylinder (in the above picture a cross-section is presented) to avoid relative displacement between the disks and to reach high geometrical tolerances in the final assembly (<10um).

To mitigate the project risks, in case the REBCO bulks would have not been compatible with the quality and reproducibility requested to an undulator in a modern light source, a sample concept equipped with REBCO tapes has been designed and assembled. Tapes are developed to simplify the application of this very promising compound into actual coils. Their thin steel substrate (<100 um) introduces the flexibility which is missing in the bulk form while increasing their mechanical strength, towards tensile stresses. This comes with a penalty in the engineering current density (i.e., the overall current density) which is only partially mitigated by the superior J_c in the superconductor with respect to bulks. For our application the tapes can be stacked to constitute a composite bulk as suggested in [12]. The stacking procedure implemented is presented in Figure 8, where the main steps are illustrated.

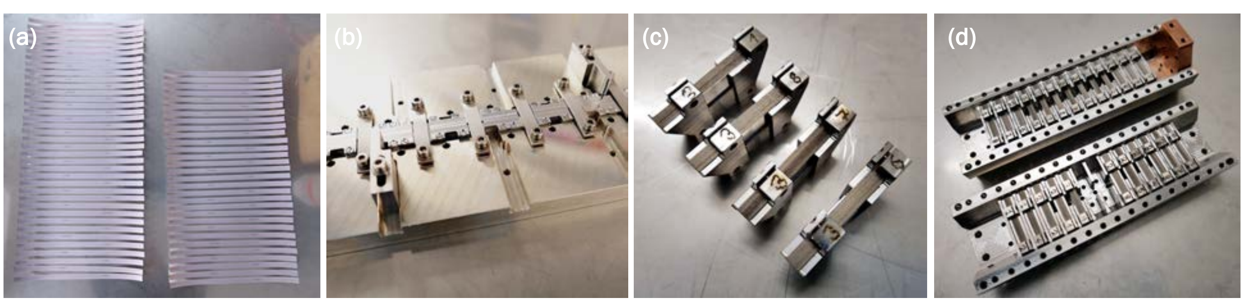

Figure 8 (a) REBCO tapes before stacking (b) Stack of tapes clamped in shells for cutting (c) Single stacks of ReBCO tapes (d) ReBCO stack assembled into a staggered array.

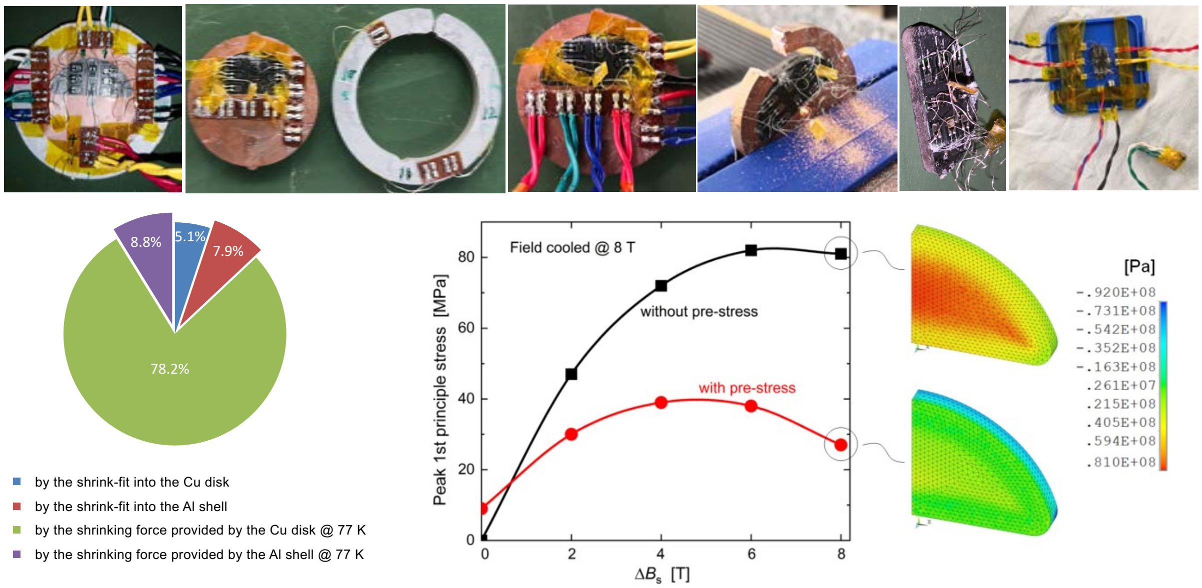

Figure 9 On the top the sample used for the strain measurements during the different steps of the assessment, on the bottom the summary results where a substantial reduction of the peak 1st principle stress is presented by calibrated ANSYS simulations.

4.1 Strain measurements

To minimise the peak tensile stress (1st principal stress) in the ReBCO bulk superconductor and prevents a premature quench during FC magnetisation, we have proposed a novel shrink-fit assembly technique and first adopted it in one single YBCO-Cu-Al piece. To characterise the mechanical strains in the YBCO bulk and evaluate the pre-stress contribution from the copper sleeve and the aluminium shell, an inverse measurement method is proposed as shown in Figure 9. It can be concluded that most of the compressive mechanical strain comes from the shrinking force provide by the copper sleeve at 77 K while the two shrink-fit assembly steps and the shrinking force provided by the aluminium shell at 77 K contribute little. The most affective structure element is the copper sleeve, while the Aluminium cylinder is not strictly required, relaxing constrains on the final design, where different criteria can be used, like for instance the heat conductivity to improve the cooling of the insert. Figure 9 also shows the simulated peak tensile stress in the pre-stressed YBCO bulk which drops from 82 MPa to 39 MPa, a safety value. Two 10 cm long industrial HTS samples were then fabricated by assembling twenty 4.0 mm thick shrink-fitted YBCO-Cu pieces and twenty 1.0 mm thick copper pieces into a 10 cm long aluminium shell with transition fits. To validate the aluminium shell is in close contact with YBCO-Cu pieces in cryogenic environment, twenty strain gauges are mounted on the outer surface of the aluminium shell and two compensation strain gauges are mounted on a small stress-free aluminium block as shown in Figure 10a; after cool down to 77 K, the thermal strains of the aluminium shell are compensated and the recorded values are net mechanical strains. Figure 10b plots the measurement mechanical strains after each thermal cycle at 77 K. It can be found that all strain values are positive which means the aluminium shell experiences tensile hoop stress along the axial length and the copper sleeves are compressed by the aluminium shell at 77 K. This proves well that the transition fit between the 10 cm long aluminium shell and forty copper sleeves is a feasible solution.

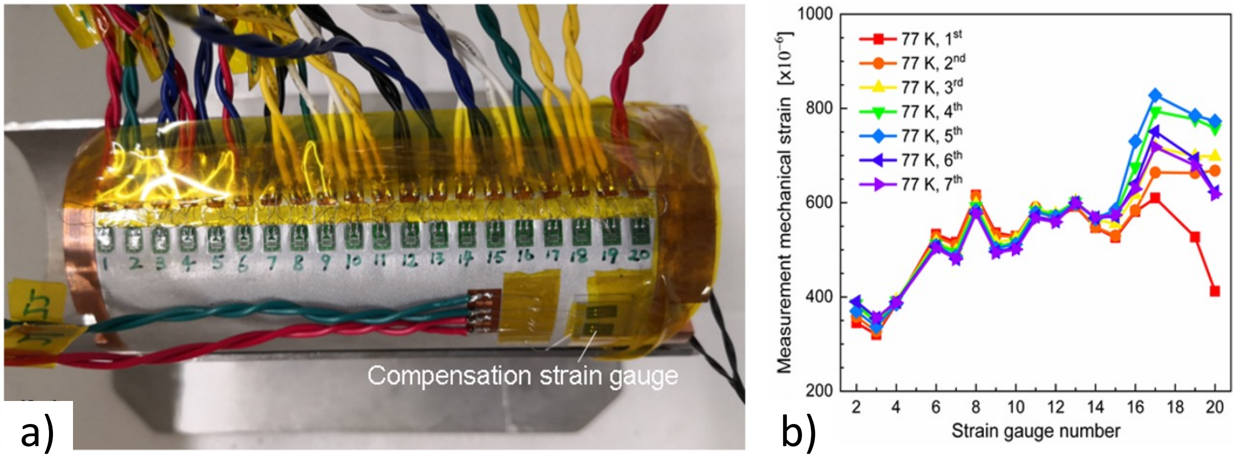

Figure 10 (a) 10-cm long HTS sample with mounted strain gauges; (b) measurement mechanical strains after thermal cycle trainings.

Additional experiments were carried with neutron beam at the ZEBRA beamline of PSI. Measuring the intensity of a diffracted neutron beam on a crystal as a function of the out-coming beam angle (2θ), gives information on the atomic spacing and consequently to the strain if stress is applied. At this beamline it is possible to control the temperature as well and the magnetic field, which allows to reproduce (on a small sample) the same operating conditions of the crystal in the undulator and to measure the strain and calculate the stresses. An example of raw data is presented in Figure 11 where the counts on the detector are recorded as a function of the angle. This technique is very promising but additional tests need to be carried out to evaluate the accuracy of this approach, which at the time being looks not enough for the practical purpose of our investigation. A straightforward improvement to this technique would be a change of particle, from neutrons to photons, not sensitive to the nuclear forces. Unfortunately, there is not a beamline available at PSI with sufficiently short photon wavelength to cope with our thick sample. Discussions of ESRF beamline scientists are ongoing to establish a collaboration.

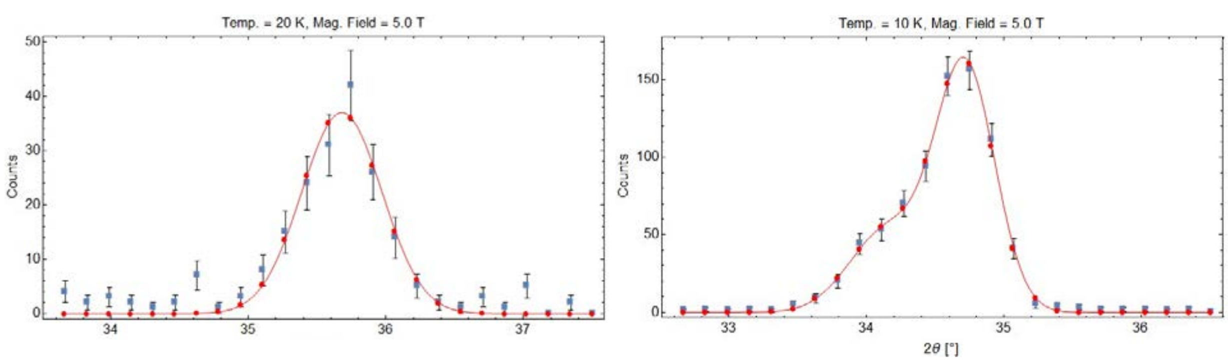

Figure 11 An example of 2theta neutron diffraction measurements on a YBCO sample.

5. Results of the Short Sample test campaigns

This experimental activity consists of the cold test of undulator samples made of 10 periods (about 10 cm long). As a project strategic decision, this activity was planned to be carried out in collaboration with the Bulk Superconducting Group of the University of Cambridge, making use to their experience and test stations.

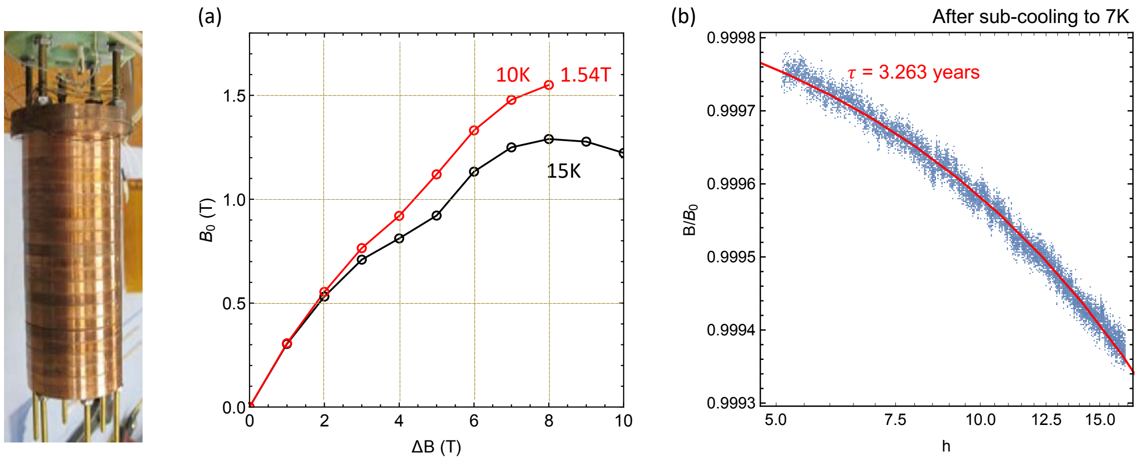

Figure 12 The test result of our best university sample, on the left (a) the magnetic field amplitude as a function of the solenoidal field variation for two different magnetization temperature, on the right (b) the flux creep after subcooling the sample from 10 to 7 K.

5.1 University samples

Two campaigns were carried out on samples of different geometries and tested in different conditions, like temperature and ramp-rate. The samples were prepared with REBCO crystals produced, machined, and assembled at the University. The first sample had the nominal period length and bulk diameter respectively of 10 mm and 30 mm and the magnetic gap of 6.0 mm larger than the nominal 4.0 mm to speed up the first testing phase when only a probe of 4 mm was originally available. The details of that measurement campaign are available in [13], where the results are presented and compared with simulations. The limitations observed in the performance due to the sudden quench closed to an on-axis undulator field of 0.85 T were supposed to be generated by mechanical instabilities because at the one hand the crystals were not permanently fixed into the copper matrix and on the other hand a small training (improving of the performances after repeating powering cycles) was observed. This interpretation was found to be most probably wrong since the reinforcement of the sample (the crystals were fixed with epoxy resin inside the copper matrix) had no impact on this phenomenon.

The second sample was prepared with the nominal geometry (4 mm gap) and tested with the novel magnetic probe of only 3 mm diameter. This sample was measured at 10 K and 15 K, and the results are presented in Figure 12a. The magnetic field amplitude achieved at 10 K is of 1.54 T, substantially higher than at 15 K, suggesting concentrating the future efforts only at this lower temperature. At the same time, the operation at 10 K was limited by premature quenches, not observed at higher temperature. Counter measures to reduce the flux creep after the magnetisation were investigated as well. Satisfactory results were achieved while lowering the temperature from 10 K (magnetisation temperature) to 7 K, recording time constant > 3.2 years, see Figure 12b.

These preliminary results identified important operational parameters which helped in focusing the efforts during the following test campaign. Nominally, the sample shall be magnetised around a temperature of 10 K with a ramp rate of 1 T/h starting from a maximum field of 10 T.

5.2 Test of the YBCO samples

The first industrially prepared sample was tested making use of the new measuring system described in section 3. The magnetic field profiles are presented in Figure 13a, two runs were carried out, the first (in blue) starting with field cooling level of 8 T and the second one (in red) with 10 T. An undulator field of 1.90 T (average value among 18 poles) was achieved for the first time. This sample was assembled with YBCO crystals from the German company ATZ[8] and precisely ground to the nominal thickness of 4+/-0.01mm, wire eroded (EDM) to their final shape (5 um accuracy) and shrank fit into copper disks. A 1 mm CoFe poles were added in between the disks. If the undulator field level achieved was very satisfactory, the spread among poles was still exceeding the specifications. Having an accurate geometry (required as well for the shrink-fit technique) better than 10 um, allows to conclude that the main problem of this sample is the quality of the crystal itself.

Making use of the inverse analysis algorithm, the average *Jc* of the individual bulks was estimated. The sample was warmed up, disassembled, and assembled following the sorting procedure and tested again. The new profiles are presented in Figure 13b where it is evident a large improvement in the field periodicity. In Figure 14, the results of this long measurement campaign are summarised. The average undulator field is presented together with the peak-to-peak variation which improved from 24 % to 7 % after sorting. To better distinguish the random errors from a systematic dipole component, the spread is evaluated before and after subtracting this latter. The results are very similar for the configuration where the solenoid is totally off and varies substantially for the sorted sample when the solenoid is active. This suggests that it could be simply related to an erroneous estimation of the offsets and/or to the Hall planar effect. Nevertheless, it is expected a non-negligible systematic dipole component in the sorted sample due to the nature of the algorithm. This value is proportional to the average variation of the *Jc* between neighbouring disks and to the total number of disks (or length).

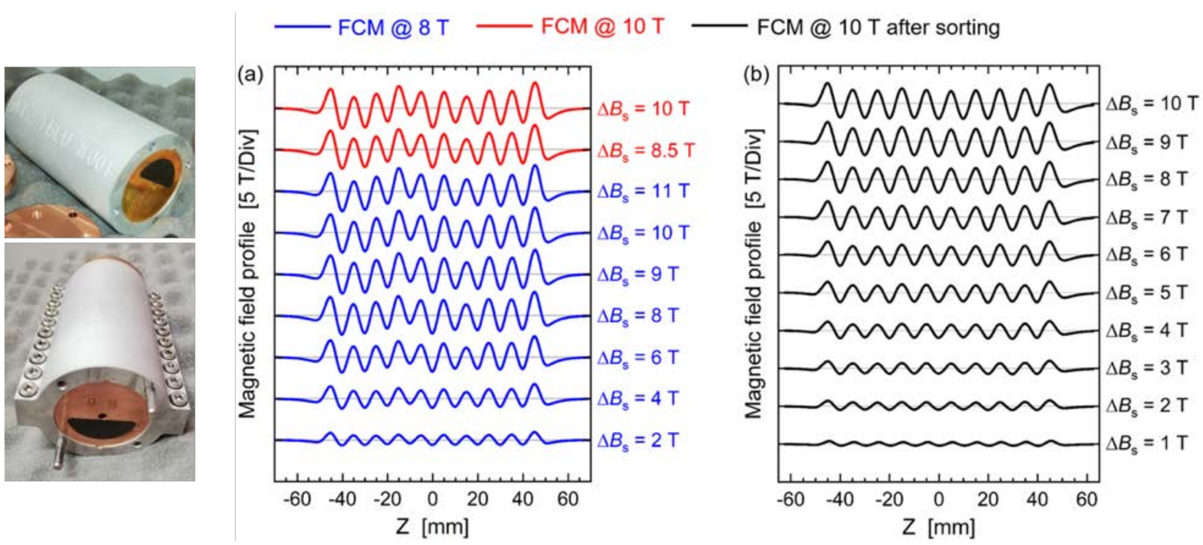

Figure 13 Measured on-axis undulator field B_y (a) before sorting and (b) after sorting. ΔB_s refers to the change in the background solenoid field.

[8] Adelwitz Technologiezentrum GmbH.

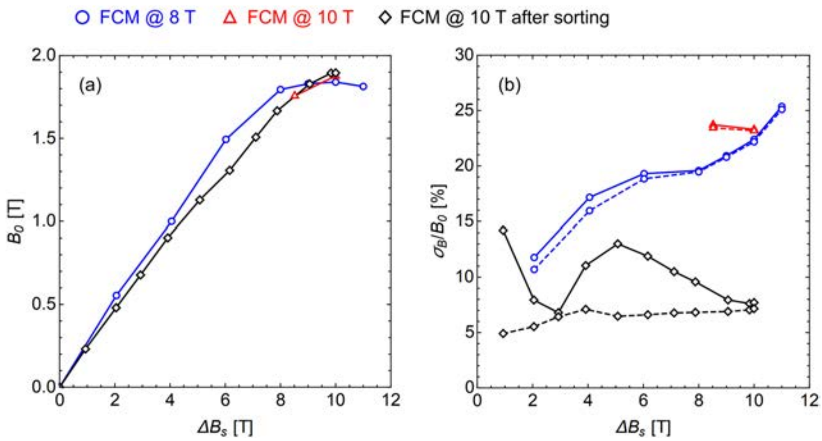

Figure 14 (a) Relation between the mean undulator field B_0 and ΔB_s. A record field of 1.90 T is obtained after sorting the bulks in the 10 mm-period undulator. (b) Relation between σ_B/B_0 and ΔB_s without correction coils (solid line) and with correction coils (dashed line).

5.3 Test of the GdBCO from Nippon Steel

With the same technique used to produce the reinforced disks, a set of GdBCO bulks from Nippon steel and CoFe poles were prepared. To simplify the assembly procedure, this time the disks were fixed between two halve shell made of copper. This latter choice was done to improve the cooling and to avoid damage to the disks, as observed while using the aluminium cylinder, probably due to the different chemical potentials. The results are presented in Figure 15, where a record field of 2.1 T was recorded together with a very low peak-to-peak variation < 3 %. This result is very similar to the performance regularly obtained with permanent magnet undulators right after their assembly. As for this latter, the actual specifications in terms of phase error can be achieved after an optimisation campaign. For this undulator the optimisation is done in the identical fashion as for the PM undulators, making used of the pole height adjustment. Of course, for this superconducting undulator, this procedure requires a thermal cycle which is time consuming. For this reason, a great effort is spent to improve the prediction capability of our algorithm for reducing the number of iterations (i.e., of thermal cycles).

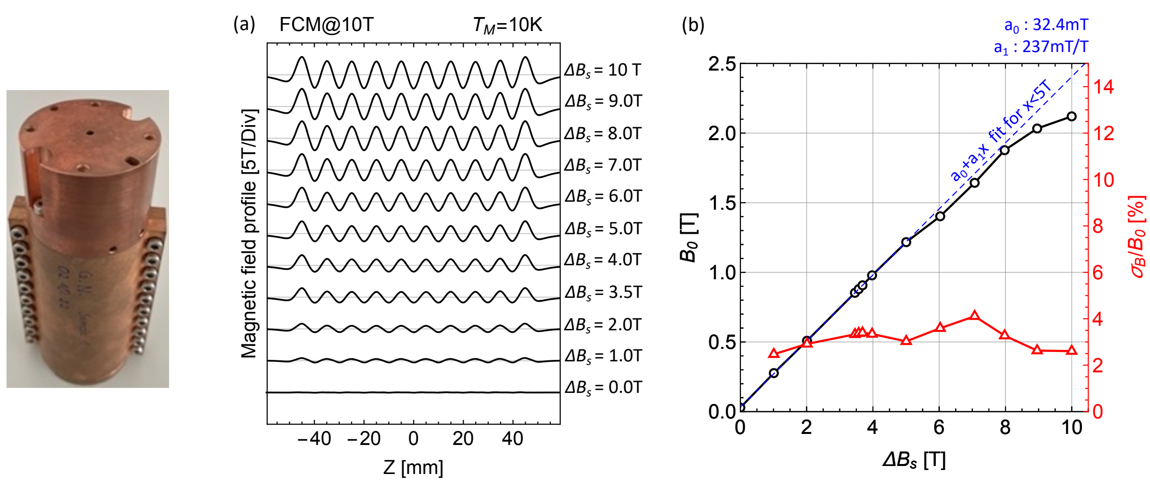

Figure 15 (a) measured on-axis magnetic field during the FC magnetization. ΔB_s refers to the change in the background solenoid field. (b) Relation between the mean undulator field B_0, σ_B/B_0 and ΔB_s. A record field of 2.1 T is obtained for a 10 mm-period undulator.

5.4 Test of the Helical configuration

Reusing the Nippon Steel series, we equipped an additional (and originally not planned) sample following the helical configuration proposed in [13]. 26 disks were used to produce a 104 mm long sample with an antisymmetric magnetic field profile. Because one period consists of 4 disks, this undulator has a longer period length of 16 mm (4x4 mm). The results are presented in Figure 16, where an effective deflection parameter ($K_{eff}^2 = K_x^2+K_y^2$) of 5.4 was achieved corresponding to a magnetic field amplitude above 2.5 T. The spread is around 3 % as expected from the previous planar undulator results. This opens a new field which the present research cannot further investigate because it is not compatible with the present schedule and budget. It is important to stress that the parameter value just achieved with this helical undulator will potentially change the design parameters of future compact free electron lasers. Project like EuPRAXIA[9] could take advantages from this new technology to further reduce the footprint of FEL facilities based on plasma laser acceleration.

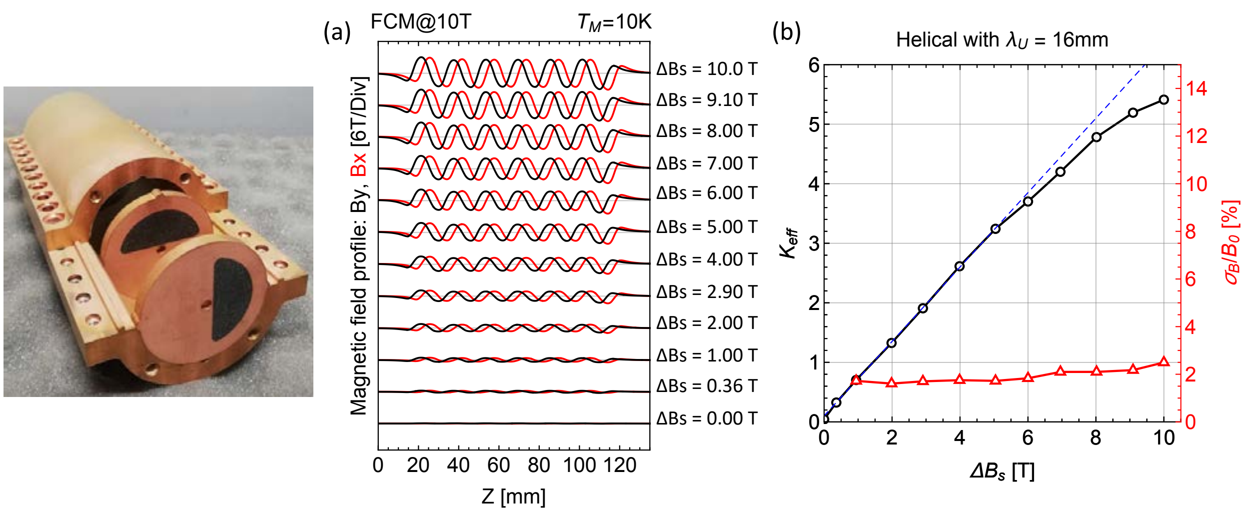

Figure 16 (a) the magnetic field profile, Bx and By, for different solenoidal magnetic field level. (b) The effective deflection parameter K and the peak-to-peak spread of the magnetic field amplitude.

5.5 Test of the tape sample

The magnetic measurement results of two stacked tape samples from different manufactures are presented in Figure 17. The THEVA sample performed slightly better than the SuperOx one, but in both cases the average magnetic field amplitude is below 0.8 T, about 60% less than the Nippon Steel sample and the peak-to-peak variation is about 8%. Implementing a set of CoFe can increase the undulator field of about 0.15 T.

Both the strength and the field quality are not satisfactory. Concerning the first, probably the estimation of the *Jc* at 10 K based on the measurements provided by both companies at 4.2 K were too optimistic. With respect to the spread, the evaluation was done based in the transport current measured along the tape by means of the TAPESTAR™[10] operated at 77 K. This parameter does not account well about the *Jc* transversal distribution which is amplified enormously by the sample geometry: for instance, if 0.5 mm at

[9] http://www.eupraxia-project.eu

[10] https://www.theva.com/products/#tapestar

the edge of the tape (on the side of the beam axis) is damaged, this results in a variation 4% of the total *Jc* but it accounts for more than 25 % of the undulator field variation. Even if the tapes production is very smooth and the stacking process is naturally averaging the imperfections, this approach does not provide better results than with the more classical bulks. For all these reasons, this approach has been abandoned.

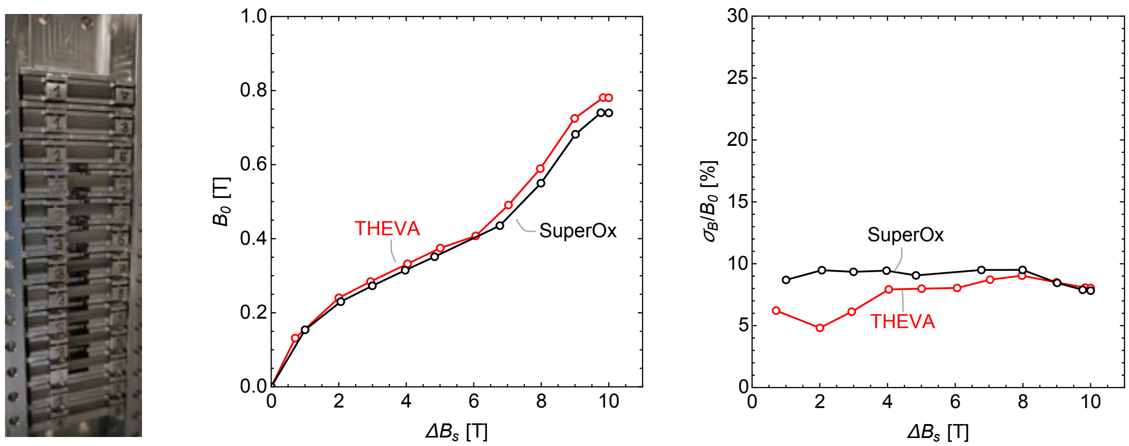

Figure 17 The summary of the two tape samples. On the left the field amplitude and on the right the peak-to-peak spread.

6. The meter long Prototype for SLS2.0

The first meter long prototype will be installed into SLS 2.0 and serve the new microscopy tomography beamline, I-Tomcat. The backbone of this device is a 12 T superconducting horizontal solenoid, 1.2 m long and with a cold bore of 100 mm diameter. This device is not readily available in the industry both because of its size and field amplitude. For this reason, its design and assembly are organised together with Fermilab. In left side of Figure 18 two views of the 3D construction drawings of the cryostat are presented, while on the right side a picture of the assembly at Fermilab on last October 2022. We choose a conduction cooling schema both for the solenoid and the HTS insert. The central cryocooler is connected to the solenoid while the two side ones are connected to the beginning and to the end of the insert.

The collaboration agreement between Fermilab and PSI (CRADA FRA-2020-0032 PSI SC Technologies) for the procurement of the 12 T superconducting solenoid was signed in September 2021. The kick-off meeting (via Zoom) was held few days later (09.09.21) where the specifications were discussed in detail once again. The coil designed is based on the last generation Nb_3Sn wire (the one developed and implemented for the High luminosity upgrade of the LHC, CERN) and any step back to more conventional conductors would require a substantial redesign and would increase the complexity of the cooling system. The choice of conduction cooling is appreciated for the absence of LHe in the accelerator tunnel but requires a coil size (coil thickness) compatible with the largest acceptable temperature gradient, easily guaranteed only with high performance conductor.

For the above-mentioned reasons, the procurement of the wire received the highest priority and the negotiation with Bruker OST (Carteret, NJ 07008, USA) was critical, since only their Rod-Restack Process (RRP®) meets the specifications. Finally, the contract was placed, and the wire was delivered 2022, in line with the time plan. With this link the authorised people can follow the regular exchange meetings, https://indico.psi.ch/category/542/.

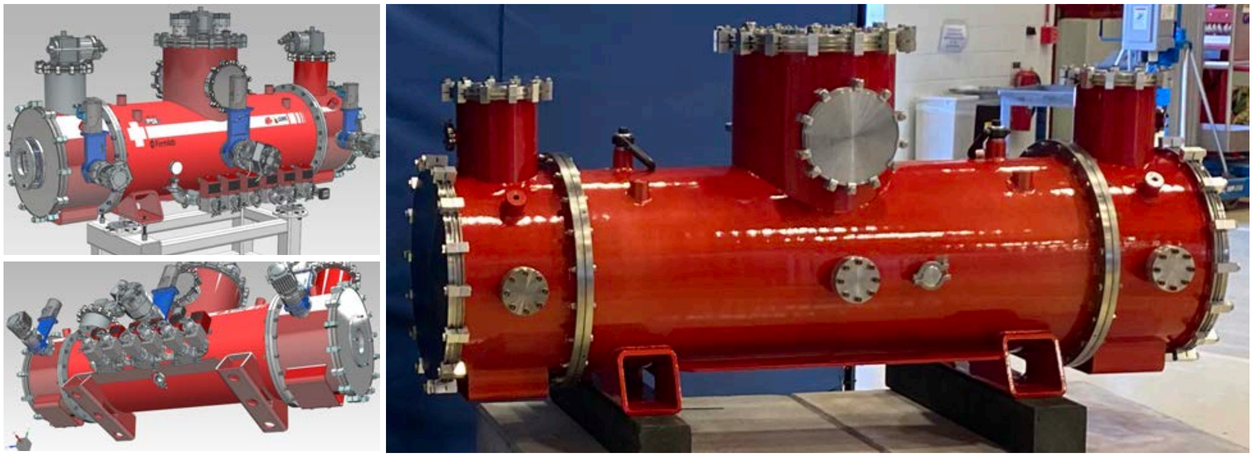

Figure 18 On the left the design of the Cryostat of the meter-long prototype done in collaboration with Fermilab. The cooling is based on conduction, powered by three cryocoolers: the central one dedicated to the superconducting solenoid and the two side ones dedicated to the HTS insert, the core of the undulator. On the right the status of the assembly on 18 Oct 2022.

6.1 Integration in the new storage ring of SLS 2.0

A preliminary study has been carried out to evaluate the compatibility of this undulator design with the beam dynamic of the storage ring. A background solenoidal field up to 4 T can be accepted only if its integral is cancelled with compensation coils and if the lattice is integrated with additional quadrupoles to account for focusing and coupling. One attractive solution would consist of two identical on axis solenoids with opposite signs, with an additional shifter in between to recover the phase when changing the undulator field. This solution would allow for an easy and fast selection of the radiated wavelength, changing the defection parameter as it is the case for conventional permanent magnet undulators. A simpler solution consists of a single solenoid operated at zero field after the magnetisation cycle. This device would not satisfy the requirement of a generic hard X-ray beamline but it fits the specification of a tomography beamline. Its reduced complexity and costs, and for the first test with beam makes it very attractive. This is the main reason why it was selected as the baseline for the I-Tomcat beamline of SLS 2.0.

Conclusions

The target values in term of magnetic field amplitude and phase error[11] were demonstrated on a 10 cm long sample making use of REBCO bulks. This was possible thanks to the novel sample preparation and to the pre-sorting procedure, avoiding the assembly of broken bulks, which degrade the field quality and cause premature quenches. The pre-stress introduced by the copper sleeves is enough to reinforce the bulks thus we avoid the assembly of the aluminium shrinking cylinder very difficult to install/remove. To fix the disks, two half-shells of copper are bolded together. This requires to manufacture them slightly smaller to guarantee an intime contact with the sleeves after the cooling down. The critical step in the

[11] The phase error measured on the Nippon samples is comparable to the one of PM undulators right after the assembly and it requires - like in the case of the PMs - several optimisation runs to achieve the final target value of few degrees. Since the procedure is identical in both cases, we preliminary conclude that this should be feasible and we will proceed in this demonstration during 2023.

sample preparation is the mechanical manufacturing accuracy requested which is below 10 um and has an impact on the total cost of the staggered array structure.

The procurement of the 12 T solenoid and its cryostat is proceeding as planned and it should be delivered in the second half of 2023. The regular exchange with the colleagues of Fermilab not only allowed a swift and customised design but improved our understanding of many technical details which would have been impossible to get within an industrial collaboration. This will simplify the future technology transfer or the creation of a spin-off company when and if this technology will be fully demonstrated in the new SLS ring.

To better account for all the efforts done in the past and ongoing today in the field of superconducting undulators, we provided an updated (up to 2022) and comprehensive summary [14] under the request of the journal SUST.

REFERENCES:

[1] XLS-Report-2019-004 27 June 2019 (https://www.compactlight.eu)[2] Billinge S J L, Levin I 2007 Science 316 (5824), pp 561-565
[3] Chupas P J et al 2003 J. Appl. Cryst. 36, 1342-1347
[4] Bertolotti F et al 2016, Nature Materials 15, 987–994
[5] Stampanoni M et al CDR TOMCAT2.0: Multiscale Multimodal Dynamic Tomographic X-ray Microscopy, PSI Internal Document.
[6] Hellmann S et al 2020 IEEE Trans. Appl. Supercond. 30 (4) 4100705
[7] Zhang K et al 2021 IEEE Trans. Appl. Supercond. 31 (2) 20169576
[8] Zhang K et al 2020 Supercond. Sci. Technol. 33 114007
[9] Zhang K et al 2021 Supercond. Sci. Technol. 34 094002
[10] Chubar O Elleaume P & Chavanne J 1997 SRI97 Conference
[11] Kinjo R et al 2022 PRAB, *25*(4), 043502
[12] Patel A et al 2018 Supercond. Sci. Technol. 31, 09LT01
[13] Calvi M et al 2020 Supercond. Sci. Technol. 33 014004
[14] Zhang K and Calvi M Supercond. Sci. Technol. 35(9), 093001